

Analysis of BPM Signal Non-linearities in CESR Vacuum Chamber

Johan Bonilla

Department of Physics, Stanford University, Stanford, CA, 94305

(Dated: August 10, 2012)

Non-linear frequencies present in fourier spectra in CESR experiments suggest the interaction of the electron cloud with stored bunches producing coupled motion referred to as Heat-Tail Motion. This is not the only explanation for the appearance of such side bands. In fact, non-linearities in the detection instruments may very well be significant enough to be comparable to what is observed. The focus of this paper is to simulate bunch positions and the signal produced onto the detection instruments in order to analyze the position fourier spectra in search of the non-linear frequencies. Results of the simulation suggest that the non-linearities of detection are strong and symmetric. This implies that the side bands can be a result of the instruments, but disparities in signal strength of frequency sign pairs ($\omega_1 \pm \omega_2$) are suggestive of extraneous effects not attributed to detection non-linearities. Also, using round beam pipes have weaker non-linearities and may serve as a test bed for Head-Tail Motion experiments.

I. INTRODUCTION

In accelerator-based experiments, such as those conducted at Cornell's Electron/Positron Storage Ring (CESR), experiment design utilizes non-invasive detection techniques. One such technique is the use of beam position monitors (BPMs) for detecting the instantaneous positions of charged bunches within the vacuum chamber. BPM signals are in the form of voltages occurring on electrodes which are translated into a scalar signal $D(x, y)$ by methods described briefly in a forthcoming section.[?]] As a result, much of the information from BPM signals can be extracted from its frequency components by means of fourier transforms. When analyzing this data, one must be able to differentiate true experimental results from background noise caused by the intrinsic properties of the experiments' instrumentation. The latter is what I will expand upon in this report.

In the case of the CESR vacuum chamber, the BPM signal is heavily dependant on the chamber's geometry. The impact of this result can be understood by considering the main contributor to the focus of CESR experiments: the electron cloud. As the charged bunches within CESR are bent in their roughly circular trajectory, they emit photons which in turn create photoelectrons off of the vacuum chamber's walls. The build-up of the electron cloud leads to non-uniform bunch motion, some of which is referred to as *head-tail motion*. [?]] The way this kind of motion is detected is through the appearance of *side bands* in the fourier spectra of the BPM position data. The problem arises when one cannot differentiate the cause of the side bands as head-tail motion or intrinsic non-linearities of the BPM signal itself. This example is just one of many experiments that depend on understanding how the instruments' non-linearities affect the data in order to accurately assess the information at hand.

II. INSTRUMENTATION

In the following section I will address an overview of bunch motion, CESR's vacuum chamber geometry, and BPM design and signal processing. Beginning with bunch motion within CESR, it is important to note that for the entirety of this paper, I will treat the bunch as a single, ultra-relativistic charged particle disregarding the accelerations from RF cavities (assume constant velocity through the ring) and suffering no influence from the electron cloud previously mentioned. The purpose of my analysis is to find the non-linearities solely due to the geometry and instrumentation, without extraneous perturbations.

A. Bunch Motion

For a traditional circular accelerator with focusing, defocusing, and bending magnets, it is known that the motion of a charged particle can be described by a superposition of betatron motion and energy oscillations.[?]] As a particle goes around the ring, different magnets provide forces that prevent the particle from deviating from the ideal orbit. It is important to note that these forces are not being continuously applied, but rather a particle encounters them in short bursts of magnetic fields leading to a roughly sinusoidal path centered about the machine's ideal orbit.

Betatron motion is analytically represented by sine-like motion that is caused by the intermittent magnet bends and quadrupoles. The true motion of a charged particle is by no means a perfect sinusoidal function, but rather described by a more complex equation

$$x(s, t) = a\sqrt{\beta(s)}\cos(\omega_{\beta}t + \phi_{0s})$$

Where $\beta(s)$ is a function which satisfies a non-linear ordinary differential equation describing the discrete magnetic interactions throughout the ring, a and ϕ_{0s} being constants determined by initial conditions, and s serves as the parametric variable describing the relative longitudinal position of the particle within the ring. At any specific point along the ring, $s = s_0$, $\beta(s)$ is constant, leaving us with

$$x(t)_{s_0} = k_{\beta}\cos(\omega_{\beta}t + \phi_{0s})$$

This makes the expression a purely sinusoid. This serves as a perfectly valid description of betatron motion at $s = s_0$ (for very much the same reason high order harmonics are indistinguishable from a base frequency in a discrete fourier transform). Since the function $\beta(s)$ is only dependant of position, if we choose a stationary sampling position, the nature of discrete sampling represents the true motion of the bunch at the location s_0 alone. As long as the betatron function agrees with all sampling points, it is a valid description of the motion at the specified location, as illustrated below in Figure 1.

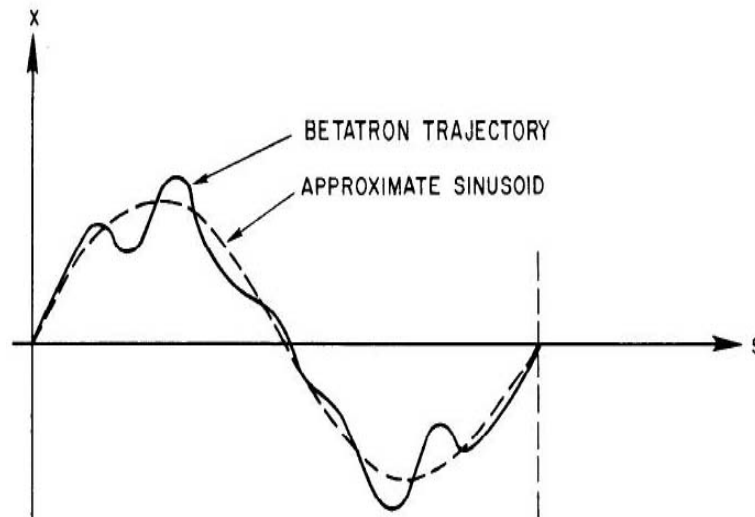


FIG. 1: Note that the motion between sampling points is unknown to the researcher. *Figure extracted from page 42 of **The Physics of Electron Storage Rings: An Introduction** by M. Sands[?]*

Betatron oscillations are present in both horizontal beam motion and in the vertical. The frequencies of these two independent oscillations are different, $\frac{\omega_x}{2\pi} = 220$ kHz, $\frac{\omega_y}{2\pi} = 230$ kHz. Apart from this disparity, there is one more major difference between horizontal and vertical motion: the energy oscillation. As a particle moves around the ring, the average energy varies from the ideal energy assumed by the machine's design. This causes the particle oscillate horizontally, traveling in an orbit of smaller radius to an orbit of larger radius and back. The reason being that any imperfection in the horizontal direction will cause a slightly larger or smaller orbit, which in turn is compensated by CESR's magnets. Take the example where it decreases its radius; this causes the particles to experience a stronger force as it passes through the bending magnets relative to a particle on an ideal orbit since it is traveling slightly faster than its outer radii neighbors. If a particle takes a smaller radius, the orbit has a smaller circumference and thus has a smaller distance to travel. This means that it speeds up relative to the ideal particle. As a result, the particle loses energy, which in turn has it experience weaker magnetic forces leading to less bending, allowing the particle to move to a larger orbital radius. Similarly, with a larger radius, the orbit is larger and the particle "speeds down" relative to its ideal-orbit counterpart. This finally causes forces that drive the particle back towards a smaller orbital radius. This behavior is branded "energy oscillation" with an angular frequency ω_s , the synchrotron frequency, which occurs dominantly in the horizontal plane by design. The equation used to describe this motion is $x(t)_s = \eta_x \delta_0 \cos(\omega_s t + \phi_{0s})$ where η_x is a machine-designed orbit dispersion function and δ_0 is a dimensionless parameter describing the peak amplitude of the oscillation. For very strong disturbances, the motion can be dampened, but there will always be a dispersion of energy within the bunch causing oscillations orbital radii.

Finally we can write our bunch motion using two equations describing the horizontal and vertical motion separately:

$$x(t) = x_0 \cos(\omega_x t + \phi_{0x}) + \eta \delta_0 \cos(\omega_s t + \phi_{0s}) \quad (1)$$

$$y(t) = y_0 \cos(\omega_y t + \phi_{0y}) \quad (2)$$

B. CESR Geometry and BPM Design

One of the most commonly found nuances in experiments conducted with CESR is related to the complexity of the vacuum chamber's geometry. For most of the length of the storage ring, the vacuum chamber lacks a simple analytic function suited to describe the shape of the pipe and be used in simulations of experiments. For this reason, it is common to approximate the geometry of the CESR vacuum chamber to an ellipse or a similar simple shape. In my analysis I used an ellipsoidal geometry to mimic the dimensions of actual CESR beam pipe as shown in Figure 2.

Beam Position Monitors on CESR are housed in flat, circular blocks, two per block and two blocks per assembly (Figure 2). Signals from BPMs are a result of the build-up of charge on the surface of the "buttons." The signal, denoted $D(x, y)$, can be simulated given the electric field produced by a charged particle. In CESR's geometry, the electric field produced by a bunch passing by is not easily obtained and must also be approximated by simulation. The process for doing so will be described in a forthcoming section. Note that in the proposed geometry the "dimples" formed towards the center make a somewhat horizontal, flat region. This region is used to simulate the flat cut-out created by the BPM blocks in the physical machine.

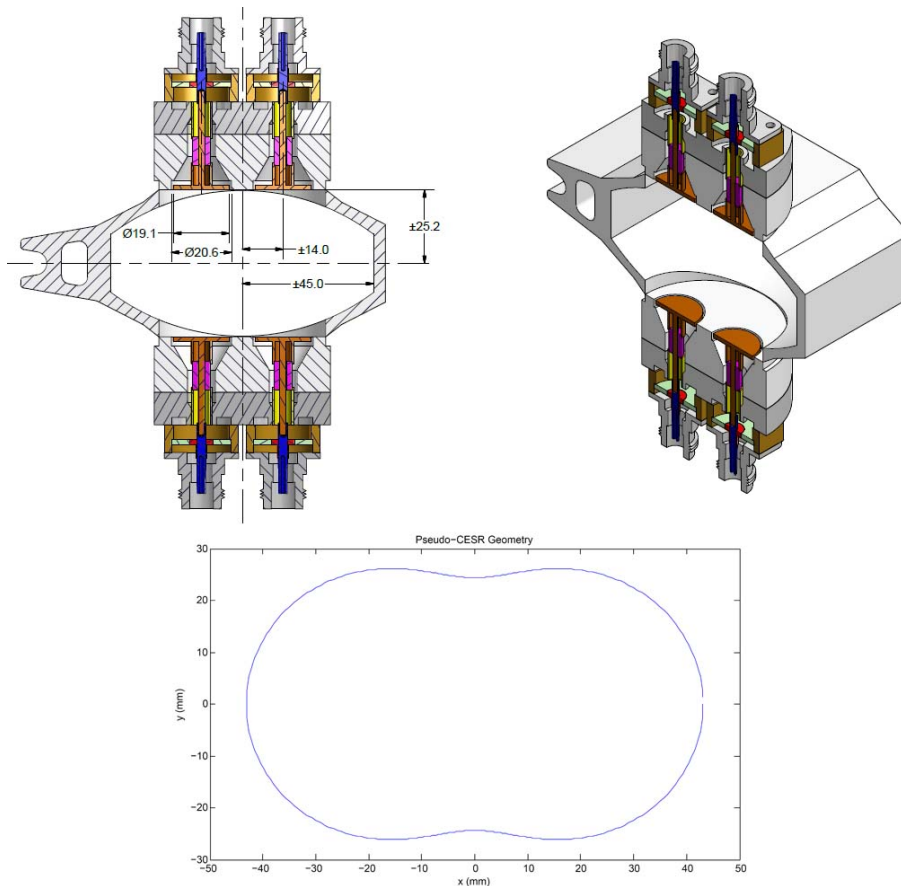


FIG. 2: **Top Left:** Cross-section of CESR vacuum chamber. Note two BPM blocks on the top and bottom walls. **Top Right:** Perspective of CESR vacuum chamber. Note flat circular cut-outs where the BPMs (gold) sit. **Bottom:** Simulated CESR vacuum chamber. Height: 52 mm, Width: 86 mm. All measurements on drawings are in mm.

[?]

III. SIMULATION DESIGN

Referring back to Eqns.(1-2), the betatron and energy oscillation functions rely on peak amplitude parameters x_0 , y_0 , and $\eta_x \delta_0$. These three parameters indicate the maximum amplitudes of each component of the motion. In practice, the energy oscillation peak amplitude, $\eta_0 \delta_0$, is determined experimentally by looking at data from exciting the bunches with longitudinal kicks produced by varying the phase of the RF cavities and recording the machine's η_x value. As a result, the value of our energy oscillation peak amplitude came from a recorded experiment, that of a CESRTA Project experiment labeled Data Set 166.[?]

Peak amplitude values for the horizontal and vertical betatron oscillations are chosen a very different way. Similar to the energy oscillation value, it begins with experimental data. Betatron motion fairly familiar and well documented. This lead researchers to develop an empirical formula relating the conditions in CESR to the RMS of the motion. For a given an average beam current (I_b) and two physical machine-given constants (x' , y'), we can use the spectrum of the position to translate the amplitudes of the horizontal and vertical spectrum

analyzer amplitudes (A_x, A_y) to determine x_{rms} and y_{rms} using the following equations:

$$x_{rms} = \frac{x'}{I_b} 10^{\frac{A_x}{20}}$$

$$y_{rms} = \frac{y'}{I_b} 10^{\frac{A_y}{20}}$$

A. Data Set 166

One of the main motivations of this project is the data from a CESRTA experiment, Data Set 166, shown below as Figure 3. The graphed spectrum displays midrange frequencies such as the horizontal betatron frequency ($\omega_h = 2\pi 220\text{kHz}$) and the vertical betatron frequency ($\omega_v = 2\pi 230\text{kHz}$), as well as "side bands" of mixed frequencies such as $\omega_v + \omega_s$ ($2\pi 255\text{kHz}$) and $\omega_v - \omega_s$ ($2\pi 205\text{kHz}$) for the last bunch in a train of 30 bunches under the influence of the effect from an electron cloud.

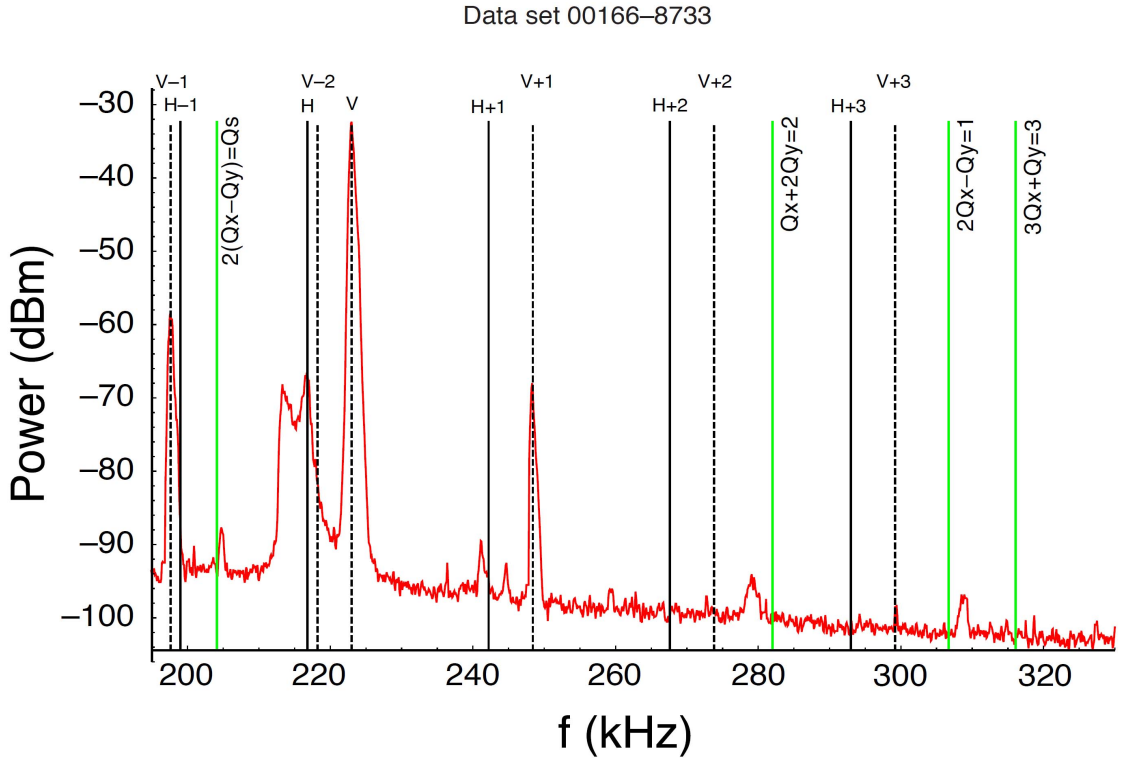


FIG. 3: Position FFT Spectrum for CESRTA experiment: Data Set 166. Shown above is the position spectrum for the 30th bunch in a 30 bunch positron train in CESR.[?]

Within CESRTA, there is a significant amount of work done that suggests some of these mixed frequencies ($\omega_v \pm \omega_s$) may be a result of Head-Tail Motion, an effect originating from a build-up of an electron cloud within the CESR vacuum chamber perturbing the charged bunches. As a bunch goes around CESR, the bunch as a whole moves in an up-down fashion at the vertical betatron frequency Fv . Then, within the bunch, different particles have different energies, which deviate with a fraction energy error δ from the ideal energy

E_0 . Particles that are at a radius within the ideal have energy $E < E_0$ travel a shorter distance around the ring, making them gain velocity relative to the ideal particle in the center. The opposite is true for particles with energy $E > E_0$. This has the particles rotate around the center of the bunch at the synchrotron frequency F_s as illustrated in Figure 4. Finally, if there is an asymmetric perturbation of the bunch, it will "wobble" and cause the motion to couple the up-down movement to the rotation. This manifests itself in the motion spectrum as the side bands, $Fv \pm F_s$. In Figure 3 we can see a significant signal at these frequencies, but it is not enough to say that it is due to Heat-Tail Motion because an alternative explanation places the cause due to the intrinsic non-linearities of the BPMs.

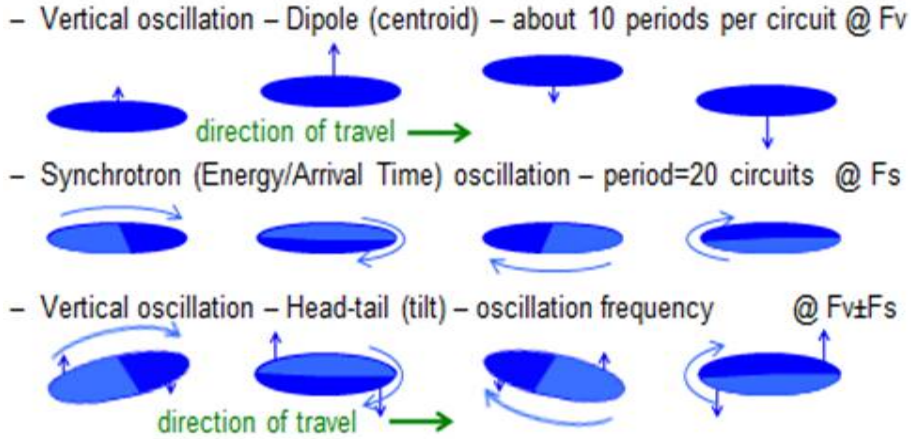


FIG. 4: Head-Tail Motion: External perturbances from the exterior such as a build-up of an electron cloud in the vacuum chamber leads to "wobbles" in the vertical position of the head of the bunch with respect to the tail of the bunch and thus the bunch precesses at frequencies $\omega_v + \omega_s$ and $\omega_v - \omega_s$ [?]

In order to test these competing hypotheses, we decided to simulate bunch motion and the associated BPM signals. As mentioned in the previous section, it is possible to find adequate parameters to simulate bunch positions such as those contributing to Data Set 166 using the frequency spectrum of previously recorded data. Looking at Figure 3, we can see that the amplitude of Fv is about -32 dB while the amplitude of Fh averages to -67 dB. Using these amplitudes and using the other physical parameters for the BPM used in the experiment, we find :

$$x_0 = \sqrt{2}x_{rms} = \sqrt{2} \frac{81.3}{.73} 10^{\frac{-67}{20}} \approx 70 \mu m$$

$$y_0 = \sqrt{2}y_{rms} = \sqrt{2} \frac{45.3}{.73} 10^{\frac{-32}{20}} \approx 2.2 mm$$

The peak energy oscillation in Data Set 166 is estimated to be on the order of $\eta_x \delta_0 = 2.7 mm$. This gives us enough information to simulate betatron motion in both horizontal and vertical directions as well as the energy oscillation term.

B. Conformal Mapping

The electric field and equipotential lines are orthogonal by definition. At any boundary of a conductor, we can say there is an equipotential line on the conducting inner surface itself.

We also know that the electric field at that boundary is orthogonal to the surface and also that we can use *stream functions* to describe the field.[?] Suppose we have a conducting surface like that of CESR's vacuum chamber. If there is a charged particle inside, there exists an electric field that permeates the space within the pipe and terminates orthogonal to the walls of the pipe. Parameterize the electric field as a stream function on the complex plane; we can couple the function describing the equipotential surface to the stream function by having the stream function U be the real part of a complex function $W = U + \iota V$ with V describing the points of equipotential as $V = \text{constant}$.[?] By the properties of conformal transformation (Riemann's Mapping Theorem) we know that we can map this geometry into any other simply connected geometry using only conformal transformations.[?] As a result, if we map the equipotential surface, the stream functions are still orthogonal to it. Previously, I presented a simulation of CESR's vacuum chamber without describing how or why this type of geometry was chosen (Figure 2). The simulated "Pseudo-CESR" geometry is made by mapping a circle of radius 15 (mm) using three conformal transformations. Beginning with the circle, we first applied an inversion transformation ($z = x + \iota y$):

$$T(z) = \frac{\alpha^2}{z}$$

For this first transformation we used $\alpha = 2.2$. The next transformation is a variation of Joukowski's transformation by replacing $+$ with $-$:

$$T(z) = z - \frac{a^2}{z^2}$$

In this transformation, $a = 1.7$. Finally, our third transformation is the same as the first, but with $\alpha = 3.17$ instead. This leads us to our final product, again illustrated in Figure 2.

Now suppose we have a series of points within the Pseudo-CESR geometry representing the various passes of a positron bunch. Use the inverse of the three transformations (and in reverse order), we can map our Pseudo-CESR geometry back to the original $r = 15\text{mm}$ circle. Similar to when we transformed the surface, we are now also transforming the stream functions lying orthogonal to the new round pipe. Were we to integrate the stream function over the entire CESR pipe, we would find the total surface charge. By properties of conformal transformations, this integration, if conducted over the transformed geometry, should be invariant. If we were to choose two points A and B , integrate the stream function between these two points, we can obtain the fraction of surface charge present between the points. Again, regardless of which geometry is being evaluated, as long as we keep track of the points and transform them accordingly, the integration of the surface charge is insensitive to the geometry. The significance of this result becomes clear when we try to find an equation for the electric field in the CESR geometry. As can be quickly deduced, it is not trivial, but if we map to the circular geometry, the problem becomes familiar and is easily solved by the method of image charges.

C. Calculating Signals

BPMs in essence are very much like guitar pick-ups. They are conductors connected to wires which send signals whenever charge moves on their surfaces. In our simulations, we determine the fraction of surface charge present on a BPM button and use this output as

the signal $D(x, y) = \frac{\epsilon_0}{\lambda} \int_{pickup} \vec{E} \bullet \hat{n} dL$, where λ is the line charge density. Using method of images we can replace a point charge in 2D space with a 3D line charge yielding the same answer. Since the BPM button and electric field has several intricacies that keep us from describing it easily in full, we will approximate the button of radius R as being made up of n smaller sub-buttons of width $w_{step} = \frac{\sqrt{\pi}R}{n}$ totaling the same area as the original BPM button and the field normal to the button as being uniform throughout the smaller sub-buttons evaluated the center of each sub-button. Thus

$$D(x, y) \approx \frac{\epsilon_0}{\lambda} \sum |E_i| w_{step}$$

. As stated before, we can find the electric field in the circular geometry quite easily by method of images. First we know the potential to be:

$$\varphi(x, y) = \frac{\lambda}{2\pi\epsilon_0} \sqrt{\frac{(x - x_b)^2 + (y - y_b)^2}{(x - x_i)^2 + (y - y_i)^2}}$$

Taking the negative gradient and substituting the image charge positions with bunch positions $x_i = \frac{x_b R^2}{r_b^2}$, $y_i = \frac{y_b R^2}{r_b^2}$, we find the electric field at a position to be: (r_b =radius from bunch to position being evaluated, $R = 15\text{mm}$)

$$E_x = \frac{\lambda}{2\pi\epsilon_0} \left(\frac{x - \frac{x_b R^2}{r_b^2}}{(x - \frac{x_b R^2}{r_b^2})^2 + (y - \frac{y_b R^2}{r_b^2})^2} - \frac{x - x_b}{(x - x_b)^2 + (y - y_b)^2} \right)$$

$$E_y = \frac{\lambda}{2\pi\epsilon_0} \left(\frac{y - \frac{y_b R^2}{r_b^2}}{(x - \frac{x_b R^2}{r_b^2})^2 + (y - \frac{y_b R^2}{r_b^2})^2} - \frac{y - y_b}{(x - x_b)^2 + (y - y_b)^2} \right)$$

Cancelling λ and ϵ we arrive at our discrete BPM signal function:

$$D(x, y) = \frac{1}{2\sqrt{\pi}} \sum_{i=1}^n \sqrt{E_x^2 + E_y^2} \frac{R}{n}$$

IV. SIMULATION RESULTS

The first simulation of BPM signals used the parameters from Data Set 166 in order to debug the programs and compare the simulations to real data. Figure 4 shows a position spectrum of the simulated Data Set 166. In this figure it is clear that frequencies from non-linearities are present. Two of the most prominent ones are our side bands of interest $Fv/pmFs$. These side bands have a peak signal amplitude of about -65 dB only 20 dB below the very strong Fv peak. They are by far the strongest non-linear frequency signal. Other significant non-linear frequencies are $Fvpm Fh$ at 10 and 60 kHz, with the latter peaking at -75 dB. It is clear that the synchrotron and vertical betatron frequencies display the strongest signals, so it comes as no surprise that the quadratic and cubic harmonics of each ($2Fs$ (52 kHz), $3Fs$ (78 kHz), $2Fv$ (70 kHz), and $3Fv$ (300 kHz)) are prominent and distinctive, $3Fv$ being the smallest of all. Also any other cross-terms involving these frequencies such as $Fh-Fs$ at 194 kHz, tend to have a characteristic peaks indicating its influence in the signals.

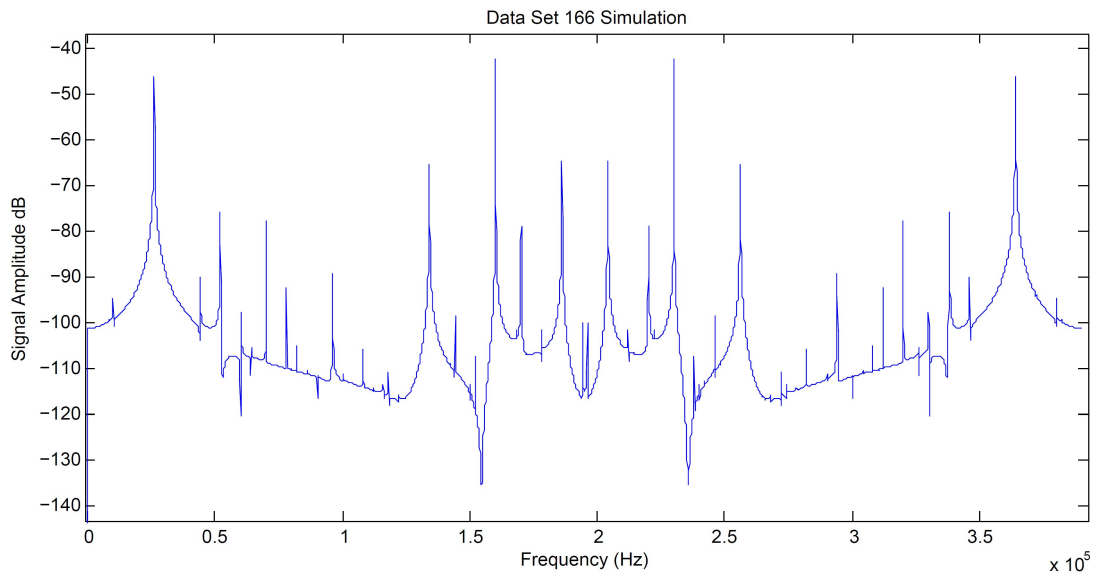


FIG. 5: Simulated Position Spectrum of Data Set 166: Note the large peaks at F_s (26 kHz), F_h (220 kHz), and F_v (230 kHz) as well as prominent side bands at 204 and 256 kHz

The cross-terms originate from the calculation of the BPM signals. Recall in Eqns. (1-2) that the positions were described as the superposition of three sinusoidal terms with different frequencies. Also, recall that in calculating the BPM signals, the positions were not only transformed, but also the electric field equation contain many different exponents which make the overall calculation very non-linear. Take the example of simply squaring the horizontal positions:

$$\begin{aligned}
 x^2(t) &= x_0^2 \cos^2(\omega_h t) + x_0 \eta_x \delta_0 \cos(\omega_h t) \cos(\omega_s t) + (\eta_x \delta_0)^2 \cos^2(\omega_s t) \\
 &= \frac{1}{2} x_0^2 \cos(2\omega_s t) + \frac{1}{2} x_0 \eta_x \delta_0 (\cos(\omega_h t + \omega_s t) + \cos(\omega_h t - \omega_s t)) + \frac{1}{2} (\eta_x \delta_0)^2 \cos(2\omega_h t) \quad (3)
 \end{aligned}$$

This illustrates how cross-terms can originate. An element of note and importance is how the different frequencies scale. Suppose we were to double the energy oscillation peak amplitude, the coefficient in front of the $2F_s$ frequency would grow as the square (quadratic growth), thus by a factor of four in this case, while the $F_h \pm F_s$ frequency would only double (linear growth), and the F_h frequency would remain constant. The next step in the simulation was looking for the growth, or lack thereof, of the different cross-frequencies by holding all but one of parameters constant.

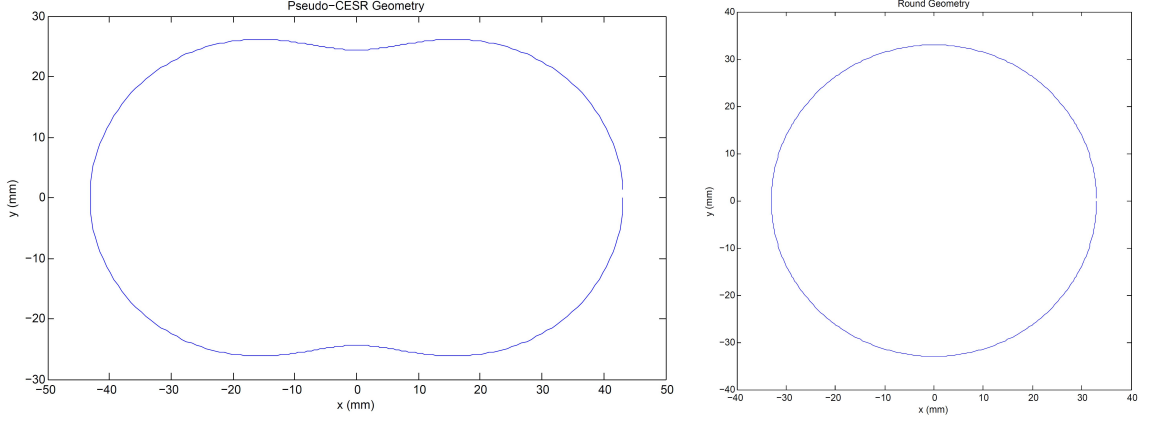


FIG. 6: **Left:** Pseudo-CESR geometry. Roughly 52 x 86 mm. **Right:** Round geometry. Diameter of 66 mm. Size was chosen by having both geometries with roughly equal area. BPMs were maintained at same positions on x-axis with same size.

A. Linear Terms

Another question that motivated this project was how much more non-linearity is present in the CESR geometry than a circular pipe. Future experiments may want to know which geometry would be ideal for certain measurements. To answer this question, we will compare the results of the BPM signal calculations in the pseudo-CESR geometry to those calculated with a circular geometry. To begin, we could note that in all of the simulations, regardless of which parameters are held constant or how big or small the peak amplitudes are made, the Fourier spectrum of the bunch positions always have a peak at the three main frequencies F_s , F_h , and F_v . This allows us to compare relative signal strength between our different geometries.

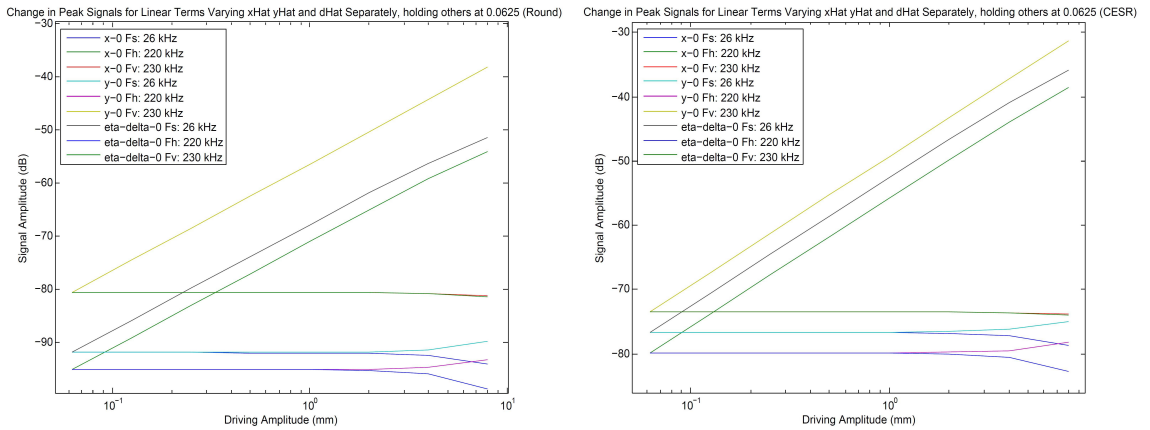


FIG. 7: **Left:** Round geometry—Vertical betatron is far greater than horizontal frequencies. **Right:** Pseudo-CESR—Overall stronger signals. Parameter being varied is shown on legend, others held constant at 0.0625 mm.

In Figure 7, we can see the three linear terms in three different situations. When the peak vertical betatron and energy oscillation amplitudes are held constant at 0.0625 mm while

varying the horizontal betatron peak amplitude by powers of 2, the signal peaks behave as expected. The horizontal betatron frequency, Fh , grows linearly, while the other two terms Fs , and Fv naturally remain constant since we forced their amplitudes to remain fixed. Note that all signals are stronger in the CESR geometry by about 10 dB, but in the Round geometry, the two horizontal frequencies are much smaller than that of the vertical betatron signal. An explanation of this comes from the BPM positions on the geometries. Though the BPM location was set to be the same size and location (on the x-axis), when applying the appropriate conformal mappings on the pseudo-CESR geometry, the BPM positions "smear" onto a greater extent on the x-axis, leading to greater sensitivity to horizontal motion in the pseudo-CESR case. Regardless of this side-note, the signals should be stronger in the pseudo-CESR case since the BPM hangs lower and thus closer to the bunches.

B. Quadratic Terms

A more interesting set of frequencies are those which mix the three principle ones. A characteristic and interesting aspect of these frequencies is how their amplitudes grow as the different parameters are varied. Take the example in Figure 8 where both the vertical betatron and horizontal oscillation peak amplitudes are held constant at 1 mm, while x_0 runs from 0.0625 to 8 mm. The most obvious line is that of $2Fh$, which has the steepest slope of all. In fact, the amplitude of the $2Fs$ peak grows at an increasing rate, arguably as a quadratic function, compared to the linear growth of Fs in the previous section. This comes as a result of the way sinusoidal terms' amplitudes scale when multiplied. From Eqn. 3, note that the coefficient in front of $\cos^2(\omega_x t) = \frac{1}{2}\cos(2\omega_x t)$ is squared. Thus, when x_0 is increased, the amplitude on $2Fs$ grows quadratically. Also, observe that the cross-terms with Fh grow linearly, while those completely lacking the frequency remain constant. Again, this comes as a result of the presence of x_0 in the coefficients corresponding to the frequencies. The exception to this is an overall increase of all of the frequency amplitudes as the varying parameter is driven harder, an effect I will dub 's'houlder growth."

Shoulder growth is the result of increasing the overall signal at a level which begins to drive the base (floor) level of the Position Fourier Transform. This can then lead to two situations, the first is that the base level will be dragged above the true signal level of some of the frequencies, burying the peaks and leading us to see the amplitude of those frequencies grow just as the base level grows. The other possibility is that strong peaks can "smear out" onto nearby frequencies and increases these amplitudes as the strong peak grows. The cause behind this is the nature of discrete Fourier Transforms. Were we to use an infinite sampling time and have an infinite amount of data, this would not exist and all peaks would be independent dirac-delta functions, but in discrete Fourier Transforms, peaks diffuse to nearby frequencies.

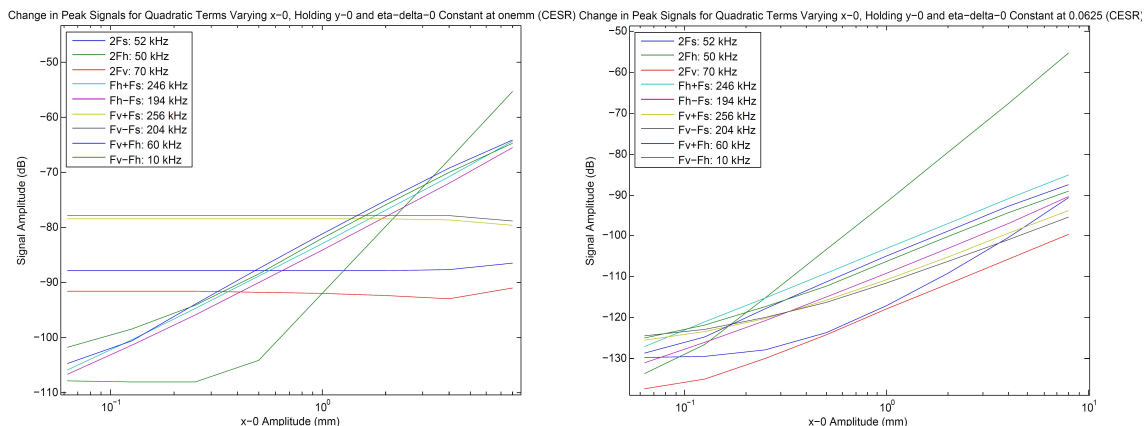


FIG. 8: **Left:** $y_0 = \eta_x \delta_0 = 1mm$; $2Fh$ grows in a quadratic fashion. $Fv \pm Fh$ and $Fh \pm Fs$ increase linearly, but terms lacking Fh remain constant. **Right:** $y_0 = \eta_x \delta_0 = 1mm$; note shoulder growth by comparing the terms that should be constant to the graph on the left.

Looking closely at the behavior of frequency "sign pairs," frequencies such as $Fh+Fs$ pair with $Fh-Fs$, we can see that either they always remain very close to each other, or they converge as the amplitudes of the frequencies increase. This is true on all of our graphs regardless of which frequency is being excited. The importance of this lies in noting that if there were side bands with different amplitudes, as in Data Set 166 (Figure 3), there is a high chance of having additional phenomena present.

V. CONCLUSIONS

The results of the simulations performed on both the pseudo-CESR and round pipe geometries can be used to interpret individual graphs and spectra, but given the motivation presented by CESRTA, I have generalized the results to three conclusions. The first of these is the convergence of sign pair amplitudes regardless of excitation levels or the frequency being varied. As noted in previous sections, frequencies pairs such as $Fv+Fh - F-Fh$ or $Fv+Fs - Fv-Fs$ tend to converge towards a mutual amplitude. If we divert our attention to CESRTA's Data Set 166 on Figure 3, we can see that there is about a 7 dB discrepancy between the side band amplitudes. Though this does not prove the presence of Head-Tail Motion, it does indicate the presence of some effect not due to BPM signal non-linearities.

The second conclusion is a result of the smaller cross-term BPM signal amplitude on the round pipe geometry. All of the data gathered in the simulations show that BPMs in the geometry detect the horizontal frequencies with weaker amplitudes. The relative strength of vertical to horizontal frequencies is more attenuated in the round than in the pseudo-CESR geometry. This tells us that the synchrotron frequency and the cross-terms involving Fs are smaller, suggesting that round vacuum chambers would serve as better the better testing bed for head-tail motion.

The last conclusion is an alternate way to decrease amplitudes of non-linear signals involving the synchrotron frequency—lower the dispersion constant η_x . Recall that the peak amplitude of synchrotron motion is proportional to η_x . If we were to choose experimental conditions minimizing η_x and thus attenuating Fs . This will eliminate non-linearities involving synchrotron motion, but then it brings up the question of how Head-Tail Motion is

generated. This, though, is beyond the scope of the result presented here, but will be an interesting task to tackle.

VI. ACKNOWLEDGMENTS

I would like to thank Michael Billing at CLASSE for providing guidance and support throughout the REU experience. Also the National Science Foundation and Cornell University for allowing me to perform research this summer. This work was supported by the National Science Foundation REU grant PHY-xxxxxxx and research co-operative agreement PHY-9809799

-
- [1] Sands, M.; *The Physics of Electron Storage Rings: An Introduction*, National Technical Information Service (1970).
 - [2] Billing, M.; CESRTA REU Presentation, June 5, 2012. *Multimedia*.
 - [3] Li, Y.; *CESR Vacuum Chamber and BPM Figures*. Downloaded July 20, 2012. *Electronic Copy*.
 - [4] CESRTA Collaboration; *Phase 1 Report*. Pgs. 270-315. Printed July 2012. *To be published*.
 - [5] P. Lorrain and D. Corson, *Electromagnetic Fields and Waves*. W. H. Freeman and Company, San Francisco, California, Second Edition, pp. 644-656, 1970.
 - [6] J. L. Walsh, *History Of The Riemann Mapping Theorem*. University of Maryland, pp. 270-276, 1973.